Available free online at www.medjchem.com

Mediterranean Journal of Chemistry

Mediterranean Journal of Chemistry **2020**, 10(1), 46-61

Synthesis and characterization of aluminum-based adsorbent and application in fluoride removal from aqueous solution

Jihane Assaoui *, Zineb Hatim and Abdelmoula Kheribech

Chouaïb Doukkali University, Faculty of Science, Water and Environment Team,
Laboratory "Biomaterials and Electrochemistry", El Jadida, Morocco

Abstract: A novel adsorbent was obtained by a facile precipitation method and was used for fluoride removal from aqueous solution. Mineralogical and physicochemical characterization of the adsorbent was carried out by X-Ray Diffraction (XRD), X-Ray Fluorescence (XRF), Energy Dispersive X-Ray attached to Scanning Electron Microscopy (SEM-EDX), BET Specific Surface Area(SSA_{N2BET}) analysis and Fourier-Transform Infrared Spectrometry (FTIR). The effect of various operational parameters such as contact time, initial fluoride concentration, (20-160 mg L^{-1}) adsorbent dose (1-6 g L^{-1}) and initial pH solution (3-11) was evaluated in batch procedures at room temperature (25±2°C). The results of the batch adsorption experiments proved that 24 h of contact time was sufficient for attaining equilibrium. The maximum wastewater defluoridation (84.91%) was obtained for 40 mg L^{-1} and 3 g L^{-1} of initial fluoride concentration and adsorbent dose, respectively. It appears that there was no significant effect on the F^- removal over a wide range of pH 3-11. Kinetic studies revealed that fluoride adsorption fitted well to pseudo-second-order. The adsorption isotherm of fluoride sorption indicated that the maximum adsorption capacity was noted to be 43.29 mg g^{-1}. Batch adsorption data was better described by Langmuir isotherm confirming monolayer adsorption with homogenous distribution of active sites and without interaction between adsorbed molecules. The obtained results indicated that the ion exchange is probably the main mechanism involved in the F^- adsorption by the aluminium-based adsorbent.

Keywords: Fluoride, Aqueous solution, Aluminum-based adsorbent, Kinetic studies, Adsorption isotherms.

1. Introduction

Fluoride, a naturally occurring element present in the soil, water, food and several minerals composition [1,2]. It is an essential trace element for the human body for the dental calcification enamel and maintenance of healthy bones. Furthermore, fluoride is widely used in the organic drug industry [3,4], fluorinated polymers [5,6], surfactants [7,8], battery components [9], etc. However, fluoride contamination has been recognized as a serious problem worldwide, an excess of this element can lead to ecological damage [10]. This excess is mainly due to the dissolution of natural minerals like fluorapatite and fluorite in the aquatic environment [11]. Volcanoes can also lead to the release of gases containing hydrogen fluoride into the atmosphere before its transfer to the aquatic ecosystem [12,13]. In addition to natural sources, fluoride may also be found in industrial wastes such as semiconductor industries [14-16] the metal surface treatment [17], the fertilizers production [18], the application of the fertilizers and pesticides in the agriculture, and glass manufacturing [19,20]. The discharge of these industrial effluents can lead to an increase in the fluoride level in the receiving aqueous media (ex: groundwater table) where they are transferred by infiltration which can lead to environmental and health impacts [21-24]. In fact, recent literature reports that an excessive fluoride amount can produce toxic effects in animals and plants such a way that the fluoride ions act as enzyme poisons, inhibiting enzymatic activity and interrupting metabolic processes like the glycolysis and plant protein synthesis [25].

Moreover, the high concentrations of fluoride can inhibit or increase the algae population growth and lead to a decrease in oxygen levels in aquatic systems [22]. Recently many scientific reports seem to suggest that fluoride intake may be associated with a number of human health problems [26-28], for instance osteoporosis [29,30], arthritis, bone fragility [31], brain damage [32], etc. Due to these impacts on human health and environment, a number of international regulators have issued regulations to control the fluoride levels in water [33,34]. Different processes have been studied to remove excessive fluoride from water namely, biological processes (plants or microorganisms) [35,36] and physicochemical processes such as fluidized bed precipitation [37], electrocoagulation-flotation [38,39], ion-exchange [40,41],

**Corresponding author: Jihane Assaoui*
Email address: assaoui.j@ucd.ac.ma
DOI: http://dx.doi.org/10.13171/mjc101020291172ja

Received November 14, 2019
Accepted December 12, 2019
Published January 29, 2020

electrochemical methods [42] and membrane processes (reverse osmosis [43,44],

electrodialysis [45,46], Donnan dialysis [47], nanofiltration [48], etc.). However, each of these methods presents its drawbacks, such as a long disposal time, the use of dangerous and expensive reagents [49]. Among these methods, adsorption is mentioned as the most efficient and widely used fundamental approach in water defluoridation processes [50]. It is characterized by its simplicity and availability of a wide variety of adsorbents. The adsorption capacity and adsorbents affinity are determined by the textural and physical properties as well as their surface chemical nature [51]. A large variety of adsorbents has been reported in literature, such as iron-based materials [52], kaolinite [53], bentonite [54], lignite [55], calcite [56], tri-calcium phosphate [57], hydroxyapatite [58], red mud [59], montmorillonite [60], Alumina has been reported in the literature as an active support for water defluoridation due to its sorption properties, ion exchange potential and low cost [61,62]. However, its adsorption capacity is not always satisfactory, mainly due to the small specific surface area. For this reason, the modification of its surface, by molecules having higher fluoride adsorption, has recently been investigated [63].

Our research aims at the removal of fluoride ions from aqueous solutions through adsorption by the aluminum-based adsorbent. The investigations were focused on the dynamic adsorption behavior of fluoride on the surface of the adsorbent, including isotherms studies and kinetics, in batch experiments. The significant novelty of this study is the simple preparation of a novel aluminum-based adsorbent that increases its affinity for fluorine and its stability in different pH.

2. Experimental

2.1. Materials

All the chemicals used in the present study were of analytical reagent grade. Aluminum nitrate ($Al(NO_3)_3$, $9H_2O$), hydrochloric acid (HCl), sodium fluoride (NaF), hydrochloric acid (HCl), caustic soda (NaOH) and TISAB III were purchased from Merck.

2.2. Preparation of adsorbent

Aluminum-based particles are synthesized by precipitation method [64]. Aluminum nitrate and sodium hydroxide as the basic raw material were used for the process. The uniform aluminum solution was prepared by dissolving 375,13 g aluminum nitrate ($Al(NO_3)_3,9H_2O$) into deionized water. Then, 800 mL of a 5 M NaOH solution was added. The aluminum nitrate reacted with sodium hydroxide, at room temperature, in a ratio of 1:4. The nucleophilic substitution of the OH group makes it possible to prepare $Al(OH)_4$ with sodium nitrate and water. The obtained precipitate was filtered and dried in a draught drying cabinet at 105°C for 12 h. The obtained powder was ground, sieved through 1 mm sieve, and then calcined in a muffle furnace at 750°C for 4 h in the presence of air at a heating rate of 10°C.min^{-1}. The theoretical equations for the adsorbent synthesis can be written as Eqs. 1 and 2 [64].

$$Al(NO_3)_3,9H_2O + 4NaOH \rightarrow Na(Al(OH)_4) + 3NaNO_3 + 9H_2O \quad (1)$$

$$Na(Al(OH)_4) \rightarrow Na(AlO_2) + 2H_2O \quad (2)$$

2.3. Characterization of adsorbent

An accurate structural and morphological characterization of adsorbent was determined by X-Ray Diffraction (XRD X'Pert PRO Panalatycal) and X-Ray Fluorescence (XRF, Oxfordmdx 1000). The Specific Surface Area was determined by the BET method using nitrogen adsorption (SSAN2BET) (Flowsorb II 2300, Micromeritics). Energy Dispersive X-ray attached to Scanning Electron Microscopy (SEM-EDX) was used to observe the morphological features of synthetic adsorbent and to determine the spot element analysis of these latter. The functional groups present in adsorbent were determined by FT-IR using a Fourier Transform Infrared spectrophotometer, (Model Bruker Vertex 70. FTIR) spectra were recorded between 4000 cm^{-1} and 400 cm^{-1}.

2.4. Fluoride solutions preparation and instrumental analysis

Sodium fluoride (NaF) was used during adsorption experiments as the source of F^-. A stock solution of 100 mg L^{-1} F^- was prepared by dissolving 221 mg of NaF in 1000 mL of deionized water. Experimental solutions for various experiments were then prepared by appropriate dilution of the stock solution. F^- concentration was measured by the potentiometric method [65] with a fluoride-specific ion electrode (WTW F800 Fluoride Combination Electrode) connected to a digital ion analyzer (WTW InoLab pH/Ion 7320). The use of Total Ionic Strength Adjustment Buffer III (TISAB III) [66] was for maintaining the ionic strength pH constant to decomplex Metal–F complexes present in the sample during the measurement (NF T 90-004). All adsorption experiments were conducted at room temperature of 25±2°C.

2.5. Batch adsorption experiments

The batch experiments consisted analysing the effect of controlling parameters such as contact time, initial F^- concentration, adsorbent dose and initial pH solution (the pH adjustment was carried out by using 0.1 N (HCl) or 0.1 N (NaOH)) on F^- adsorption. All the experiments were conducted at room temperature of 25±2°C in 500 mL plexiglass reactor. A specific

amount of adsorbent was added to the fluoride-doped synthetic solution. The reaction mixture was continuously blended by an electric rod stirrer at 350rpm. At equilibrium, the liquid phase is recovered in an Erlenmeyer flask after vacuum filtration through Whatman No. 42 filter paper for F^- analysis, The equilibrium study is performed by varying initial F^- concentrations from 20 to 160 mg L^{-1}, while maintaining the constant adsorbent dosage and the contact time at 3 g L^{-1} and 24 h, respectively, for each sample. The effect of adsorbent dosage is studied by varying the mass of adsorbent from 1 to 6 g L^{-1} in a sample of 40mg L^{-1} initial F^- concentration at natural pH (7±0.2). The effect of pH is also studied by conducting experiments for a variation of pH from 3 to 11 by keeping the initial F^- concentration and the adsorbent dose at 40 mg L^{-1} and 3g L^{-1}, respectively.

2.6. Fluoride removal calculation

The specific amount of the adsorbed F^-, Q_e (mg g^{-1}), was calculated according to Eq. (3):

$$Q_e = \frac{C_0 - C_e}{W} \times V \quad (3)$$

Where, Q_e is the adsorption capacity (mg g^{-1}) in the solid at equilibrium; C_o, C_e are initial and equilibrium concentrations of F^- (mg L^{-1}), respectively; V is the volume of the aqueous solution (L) and W is the mass (g) of adsorbent used in the experiments.

The adsorption removal efficiency (*ARE*), at equilibrium, was calculated by using Eq. (4):

$$ARE\ (\%) = \frac{C_0 - C_e}{C_0} \times 100 \quad (4)$$

2.7. Modeling studies

2.7.1. Kinetic models

The pseudo-first-order is a kinetic model described by the following Lagergren Eq. (5) [67]:

$$\frac{dQ_t}{dt} = K_1(Q_e - Q_t) \quad (5)$$

The linear form of pseudo-first order kinetic model can be expressed by Eq. (6):

$$\log(Q_e - Q_t) = \log Q_e - \left(\frac{K_1}{2.3}\right) t \quad (6)$$

Where, Q_e and Q_t are the amount of F^- adsorbed (mg g^{-1}) at equilibrium and at a time 't', respectively. K_1 (min^{-1}) represents the rate constant of pseudo-first-order adsorption reaction. A straight line of $\log(Q_e - Q_t)$ against t suggests the applicability of these kinetic models. Both Q_e and K_1 can be determined from the intercept and slope of the curve, respectively.

The linear form of the pseudo-second-order kinetic model can be expressed by Eq. (7) [68]:

$$\frac{t}{Q_t} = \left(\frac{1}{K_2 \times Q_e^2}\right) + \frac{t}{Q_e} \quad (7)$$

where K_2 is the rate constant for pseudo-second-order reaction (g mg^{-1} min^{-1}). Q_e and Q_t are the amounts of F^- adsorbed at equilibrium and at any time 't' (mg g^{-1}), respectively. The straight-line plot of t/Q_t against t for the kinetic data gives the values for Q_e and K_2 from the slope and intercept, respectively.

2.7.2.. Adsorption isotherms

The isotherm equations Langmuir and Freundlich isotherm models have been used in the present study, to describe the equilibrium data. The Langmuir equation can be described in the following Eq. (8) [69]:

$$Q_e = \frac{Q_m \times K_L \times C_e}{1 + (K_L \times C_e)} \quad (8)$$

The linearized form of Eq. (6) can be written as Eq. (9):

$$\frac{1}{Q_e} = \left(\frac{1}{Q_m \times K_L}\right)\left(\frac{1}{C_e}\right) + \frac{1}{Q_m} \quad (9)$$

where C_e is the equilibrium concentration of fluoride ions (mg L^{-1}), Q_e is a solid phase concentration of fluoride ions (mg g^{-1}), Q_m (mg g^{-1}), and K_L (L mg^{-1}) are empirical constants, can be evaluated from the slope and intercept of the linear plot of $1/Q_e$ against $1/C_e$.

The Freundlich is expressed mathematically in linear form as it is represented in Eq. (10) [70]:

$$\log Q_e = \log K_F + \frac{1}{n} \log C_e \quad (10)$$

Where, K_F (mg g^{-1}) and $1/n$ are Freundlich constants related to adsorption capacity and adsorption intensity, respectively. Those constants are obtained from the intercept and slope of $\log Q_e$ versus $\log C_e$ linear plot, respectively.

3. Results and discussion

3.1. Characterization of adsorbent

3.1.1. X-Ray Diffraction (XRD) analysis

The structural characterization of synthetic adsorbent was carried out by X-Ray Diffraction (XRD) as shown in Figure 1. XRD pattern of adsorbent showed three major well-crystallized phases (sodium nitrate ($NaNO_3$), sodium aluminum oxide (Na (AlO_2)) and sodium carbonate (Na_2CO_3)) with well-resolved peaks.

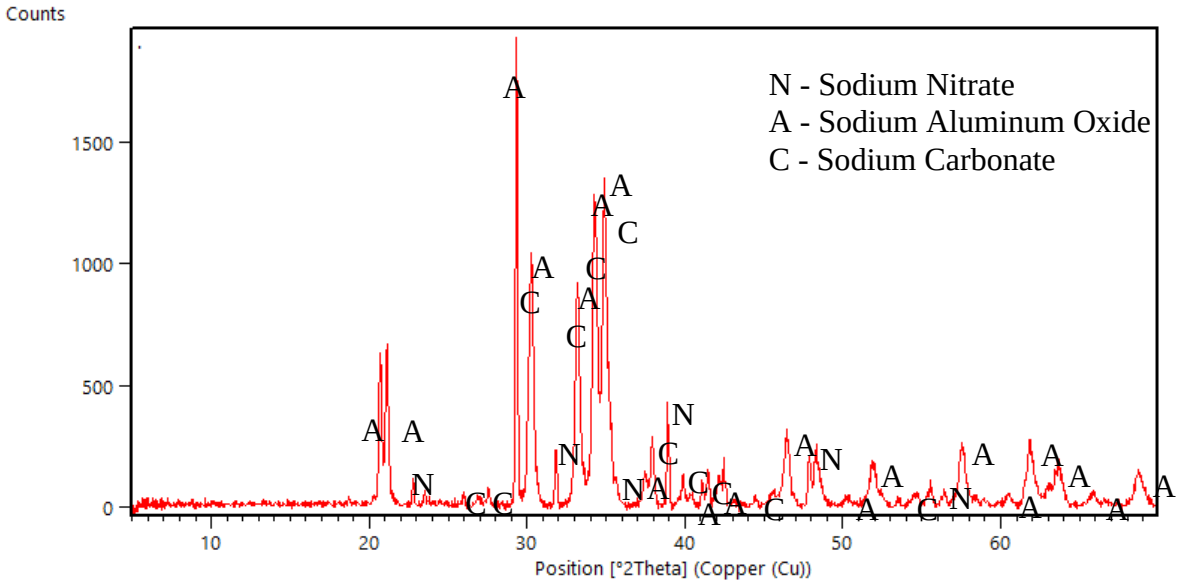

Figure 1. XRD patterns of adsorbent

3.1.2. X-Ray Fluorescence (XRF) analysis

The chemical constituents of adsorbent are shown in Table 1. The analysis revealed that alumina (Al_2O_3) was the main component at 44.97%, followed by sodium oxide (Na_2O) at 9.45%, confirming that synthetic adsorbent is based on sodium aluminum oxide.

Table 1. Elemental composition of the adsorbent.

Element	Content	Unit
Al_2O_3	44.97	%
Na_2O	9.45	
P_2O_5	0.35	
SiO_2	0.27	
CaO	0.13	
K_2O	0.12	
Fe_2O_3	533.5	ppm
Cr_2O_3	183.5	
Cl	108.8	
Ga_2O_3	20.1	
NiO	15.6	
ZnO	6.8	
CuO	6.1	
Rb_2O	3.1	
Yb_2O_3	0.6	
Re	0.5	
IrO_2	0.1	

3.1.3. Energy Dispersive X-ray attached to Scanning Electron Microscopy (SEM-EDX) analysis

The results of SEM-EDX analysis of synthetic adsorbent are presented in Figures 2, 3. The SEM pictures showed surface morphology and grain distribution.

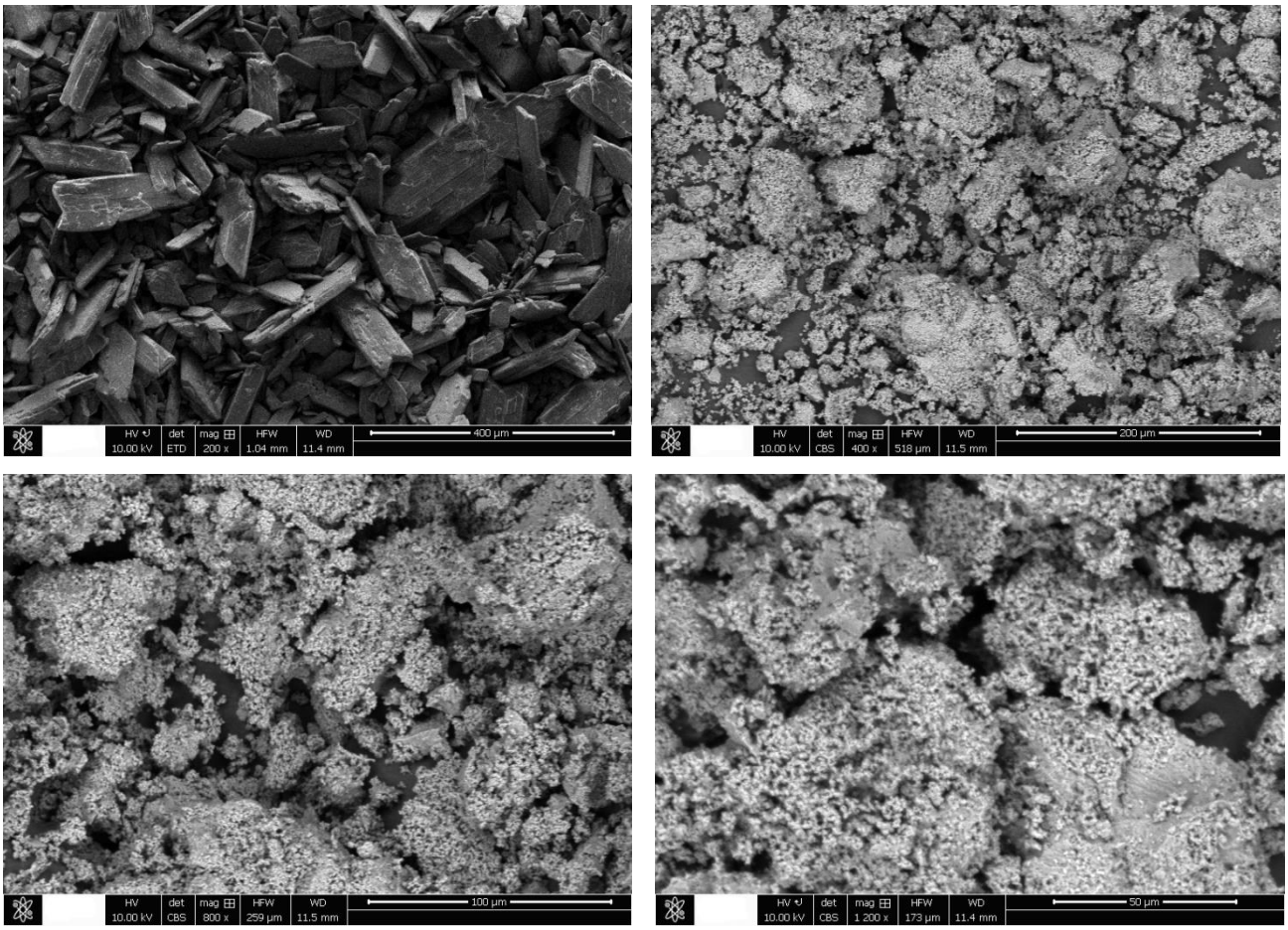

Figure 2. SEM of adsorbent

Figure 2 showed the pictures that were obtained by applying a voltage of 10KV with different magnifications. The surface has a cloudy appearance and regular shape with bright white particles probably of aluminium, displaying a cylindrical rod as a structure with different particles size [41].

The EDX spectrum implied that the composite is made up of uniformly distributed carbon, oxygen, sodium and aluminum all over the surface as shown in Figure 3.

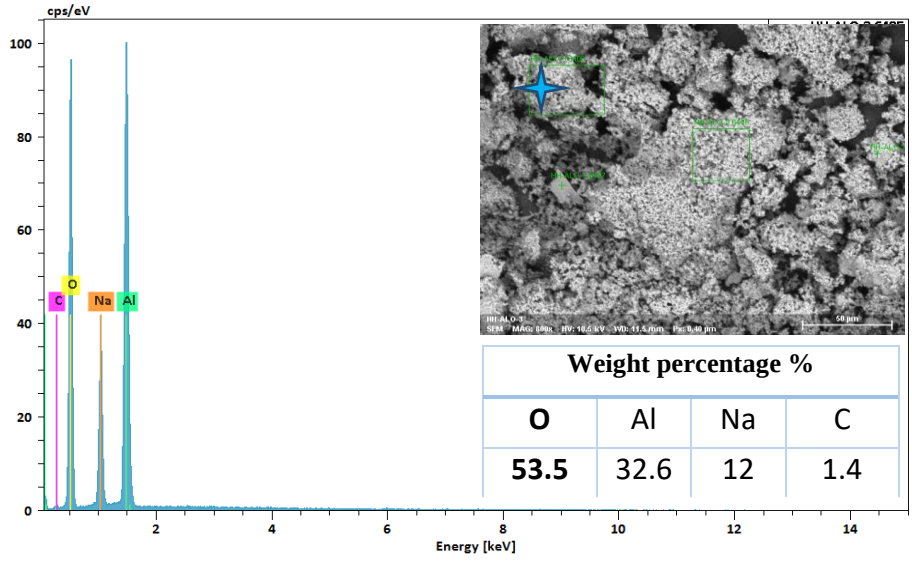

Figure 3. SEM-EDX of the adsorbent

3.1.4. BET Specific Surface Area (SSA_{N2BET}) analysis

The BET results show that the aluminum based-adsorbent presents an important surface area (≃10.0059 m^2 g^{-1}) comparing to most of the activated alumina adsorbents with some exceptions.

3.1.5. Fourier-Transform Infrared Spectrometry (FTIR) analysis

The FTIR spectra of the aluminous support, before and after adsorption (Figure 3), showed common bands corresponding to the basic structure (AlO_2) such as two bands at 1371 cm^{-1} and 1236 cm^{-1} which most probably correspond to the symmetrical and antisymmetric elongation of Al=O group. Furthermore, two bands at 966 cm^{-1} and 511 cm^{-1} correspondings to the deformations of the group Al=O [71]. While the appearance of two bands at 1742 cm^{-1} and 3428 cm^{-1} are characteristic of the OH group of the H_2O molecule. The comparison of the FTIR spectra did not show any difference between the infrared spectra of the adsorbent (Na(AlO_2)) before and after the adsorption tests. Nevertheless, if we look carefully (the spectrum in blue), we can notice that there is an appearance of small bands at 507.58cm^{-1} and 554.94cm^{-1} correspondings to the Al-F bond [72], which confirms the adsorption of F^- ions by our adsorbent through a chemisorption mechanism.

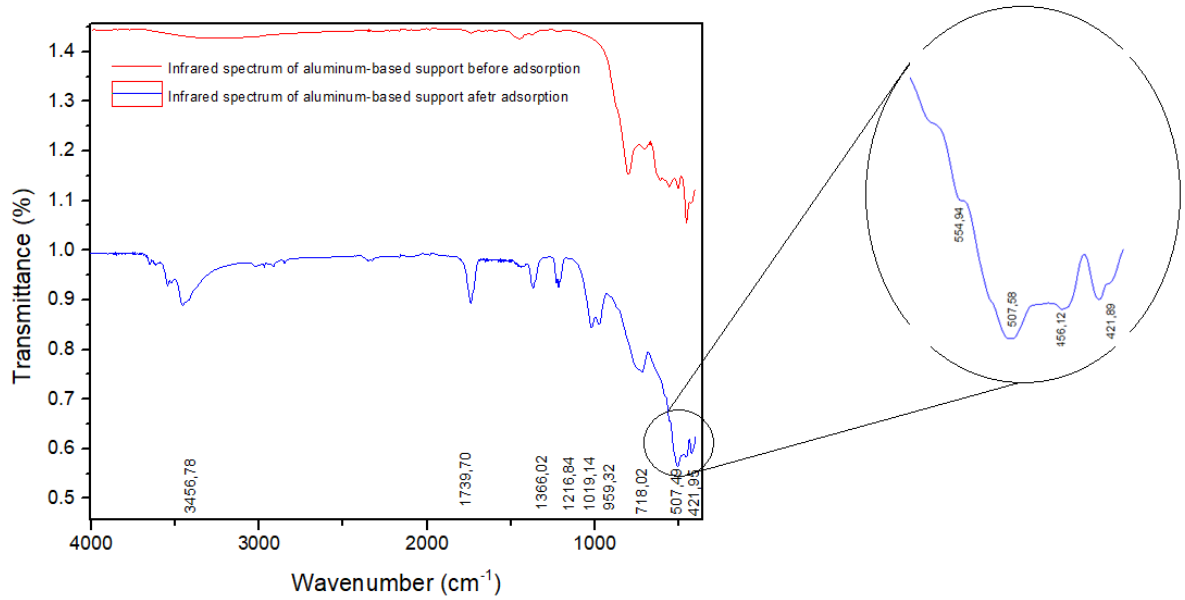

Figure 3. FTIR spectra of adsorbent and the fluoride adsorbed

3.2. Batch experiments results

3.2.1. The effect of contact time

The effect of contact time on the percentage of F^- adsorbed was investigated to ensure equilibrium state between aqueous F^- and the adsorbent.

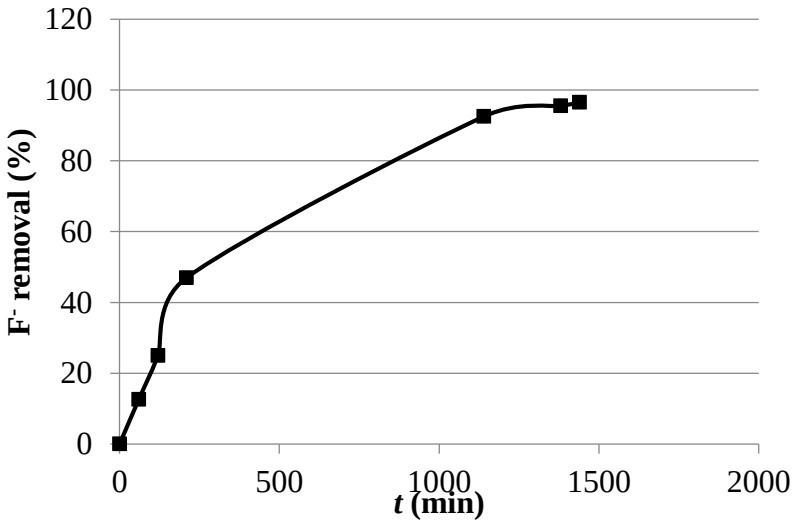

Figure 4. Effect of contact time on the percentage of F^-removal (%)

Figure 4 shows the progression of adsorption reaction, the percentage of the F^- adsorbed on to the adsorbent after different contact times. It was observed that with a fixed amount of the adsorbent, the percentage of F^- adsorbed increased with contact time and began to reach equilibrium after 24 h of reaction. Consequently, the contact time fixed for further adsorption experiments was 24 h.

3.2.2. The effect of initial fluoride concentration

The effect of initial concentration on the percentage of F^- removal was carried out to determine the maximum adsorption capacity of the synthetic adsorbent. The adsorbent dose and initial pH solution were fixed at 3 g L^{-1} and 7±0.2, respectively. As shown in Figure 5, the adsorption capacity reached stability at a high initial concentration (100 mg L^{-1}). This can be explained by saturation of the available active adsorption sites. Though, the percentage of F^- removal decreased with an increase in the initial concentration. This decrease is due to the presence of more F^- ion in solution at higher initial F^- concentration. However, the efficient F^- removal at a low initial concentration was because of the important ratio of surface active sites to total F^- ions present in solution.

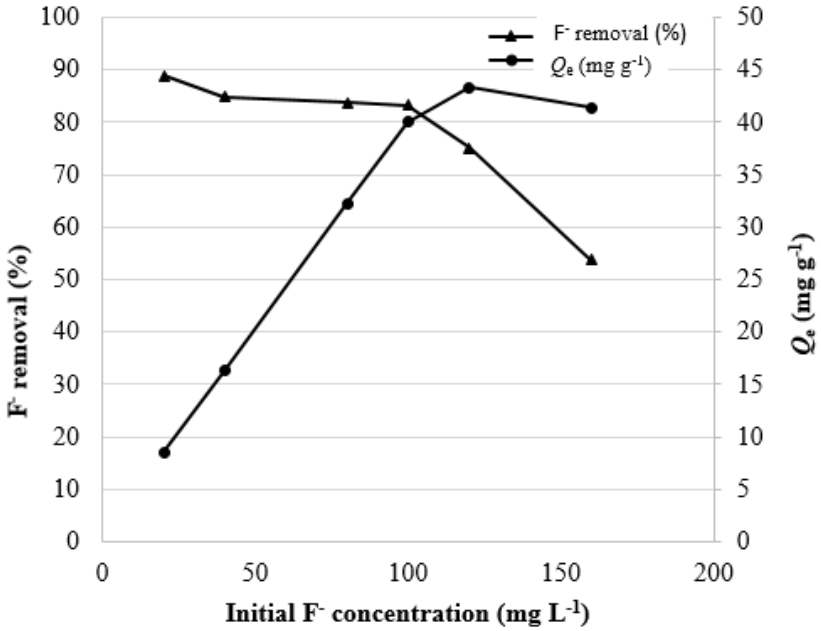

Figure 5. F^-removal and adsorption capacity against initial F^- concentration (pH =7±0.2, contact time = 24h, adsorbent dose = 3 g L^{-1}, agitation speed = 350 rpm, T = 25±2°C)

3.2.3. The effect of adsorbent dose

Figure 6 shows that the percentage of F^-removal increased slightly with increasing adsorbent dose up to 3 g L^{-1}. The increase of percent F^- removal with the increase of the adsorbent dose is due to the availability of sufficient adsorption sites. However, the addition of the adsorbent dose did not show any considerable increase in the percentage of F^-removal. This may be probably due to the overlapping phenomenon of the active sites at a higher adsorbent dose resulting in a reduction of surface area [73].

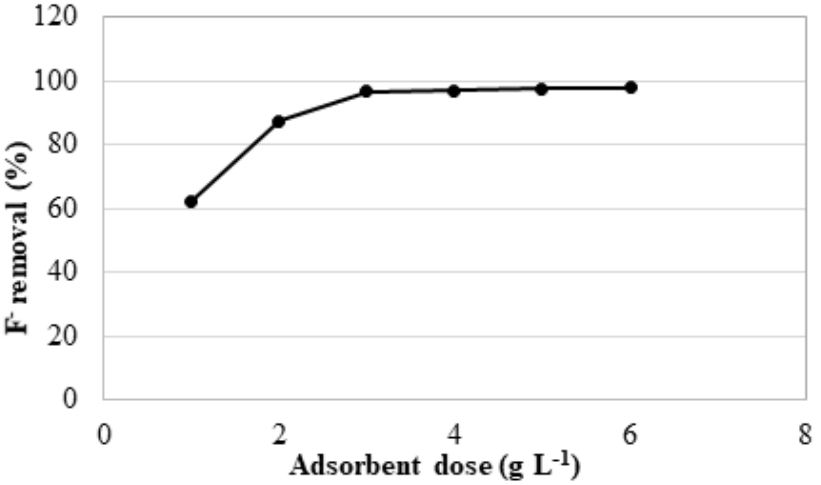

Figure 6. Effect of adsorbent dose on percentage of F^- removal (natural pH = 7±0.2, initial F^- concentration = 40 mg L^{-1}, contact time = 24h, agitation speed = 350 rpm, T = 25±2°C)

3.2.4. The effect of initial pH solution and determination of pH_{PZC}

Figure 7 illustrates the evolution of the percentage of F^- removal over the pH range of 3-11. It was observed that the percentage of F^- removal does not weaken in the full pH range of 3 to 11. The adsorption of the F^- ions on the synthetic adsorbent is thus not dependent on pH. It is therefore not simple physisorption, and there is probably an appreciable contribution of chemisorption, resulting in a partial formation of aluminum fluoride and sodium fluoride under acidic and alkaline conditions [74].

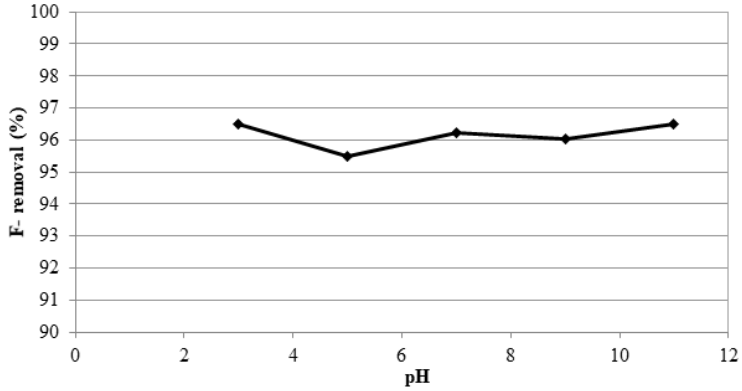

Figure 7. Effect of pH on percentage of F^- removal (adsorbent dose = 3 g L^{-1}, initial F^-concentration= 40 mg L^{-1} , contact time = 24h, agitation speed = 350 rpm, T = 25±2°C).

The point of zero charge (pH_{PZC}) plays a crucial role in determining the optimal pH of the solution where the fluoride adsorption is favored. The adsorption of these anions becomes favorable when the adsorbent surface is positively charged at a particular pH (i.e. $pH_{solution} < pH_{PZC}$) [75]. The PZC of the aluminum-based adsorbent was measured using the powder addition method [75], by adding 20 mL of 5 10^{-2} mol.L^{-1} NaCl to several 50 mL cylindrical high-density polystyrene flasks. A range of initial pH (pH_i) values of the NaCl solutions was adjusted from 2 to 12 by adding 10^{-1} mol.L^{-1} of HCl and NaOH. The total volume of the solution in each flask was brought to exactly 30 mL by further addition of 5 10^{-2} mol.L^{-1} NaCl solution. The pH_i values of the solutions were then accurately noted and 50 mg of the adsorbent was added to each flask, which was securely capped. The suspensions were shaken in a shaker at 298 K and allowed to equilibrate for 48 h. The suspensions were then centrifuged at 3600 rpm for 15 min and the final pH (pH_f) values of the supernatant liquid were recorded. The value of pH_{PZC} is the point where the curve of ΔpH (pH_f - pH_i) versus pH_i crosses the line equal to zero [76]. The obtained results are presented in Figure 8. These results show clearly that the PZC of aluminum-based adsorbent is outside a pH range of 2 to 12 because there is no intersection of the curve with the x-axis. Therefore, it can be concluded that the pH does not affect the adsorption phenomena by the aluminum-based adsorbent. This result confirms our experimental results and the pH will be no change the adsorbent capacity of the aluminum-based adsorbent.

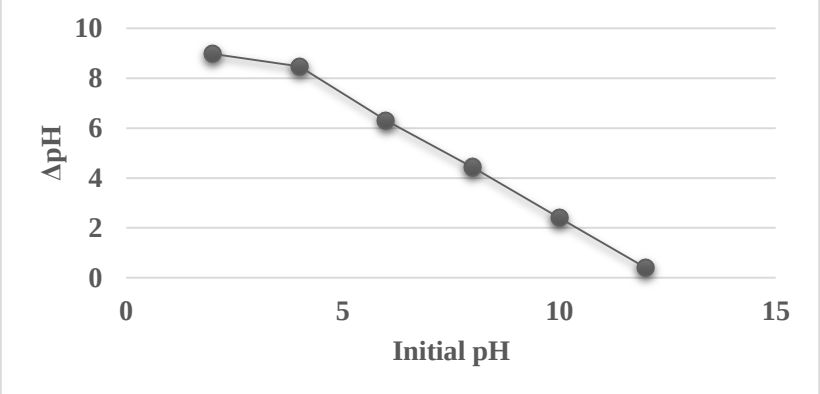

Figure 8. The determination of the point of zero charge (PH_{PZC}) using 0.05 M NaCl solutions (drift method).

3.3. Kinetic studies

Several models are exploited to fit the kinetic sorption tests [73]. In this study, the two models (pseudo-first-order and pseudo-second-order) were used to investigate the kinetics of the F^- adsorption onto aluminum-base adsorbent, in order to understand the mechanism and the rate-controlling steps affecting the adsorption kinetics. As shown in Figure 9 and 10, the pseudo-first-order (Figure 9) has a very low correlation coefficient (R^2=0.7681). Contrariwise, the pseudo-second-order (Figure 10) was found to give the best fit (R^2=0.9911)

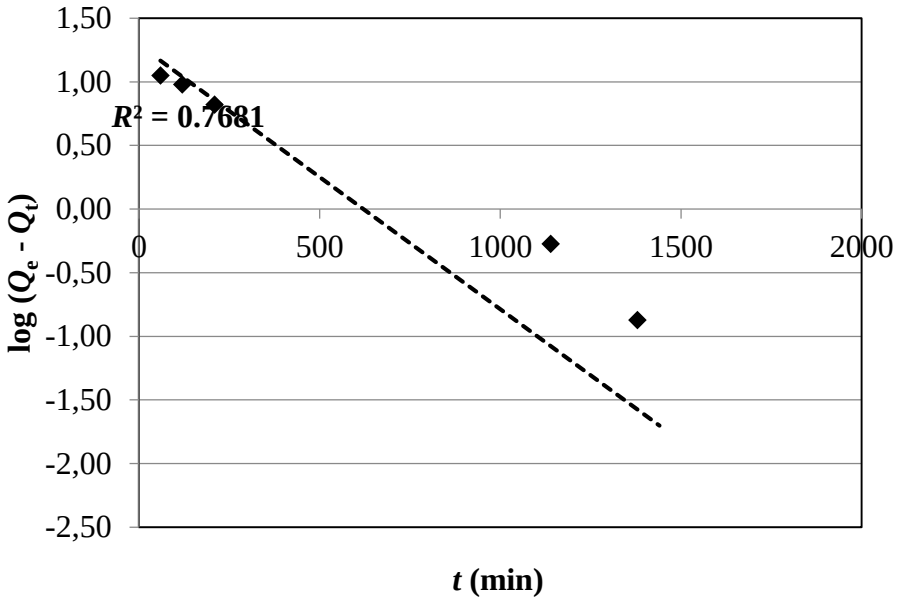

Figure 9. The adsorption kinetics of the fluoride ions on aluminum-based adsorbent according to the pseudo-first-order kinetic model.

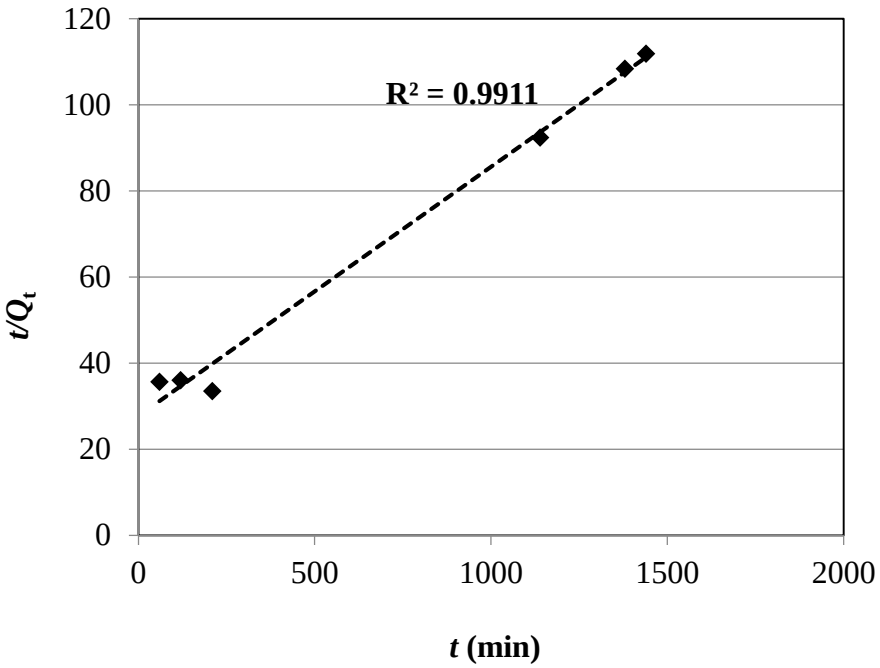

Figure 10. The adsorption kinetics of the fluoride ions on aluminum-based adsorbent according to the pseudo second-order kinetic model

3.4. Adsorption isotherm

The adsorption capacity Q_e (mg g^{-1}) of adsorbent was examined by determining the equilibrium sorption of F^- as a function of residual F^- concentration present in the liquid phase. The variation of the adsorption capacity of adsorbent for F^- is presented in Figure 11. According to the equilibrium curve, the adsorption capacity at equilibrium increases progressively at lower F^- concentration. This is because of the availability of excess adsorption sites. On the other hand, as the F^- concentration increases, the adsorption capacity at equilibrium progressively decreases until reaching saturation. The availability of adsorption sites at high F^- concentration becomes the limiting factor as the adsorbent surface reaches maximum adsorption capacity. This latter was observed to be 43.29 mg g^{-1}.

The value of the maximum adsorption capacity obtained for this study in comparison with those reported earlier for adsorption of F^- onto various adsorbents (Table 2) revealed that this aluminum-based adsorbent is an active adsorbent in removing fluoride.

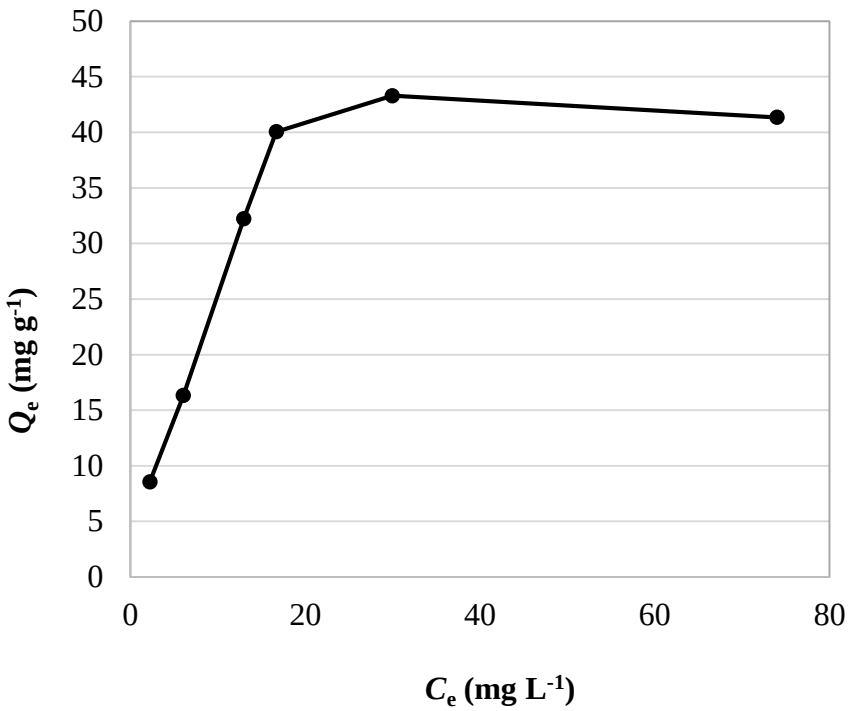

Figure11. Adsorption isotherm of F^- sorption (adsorbent dose = 3 g L^{-1}, natural pH = 7±0.2, contact time = 24 h, initial concentration = 20 – 160 mg L^{-1}, agitation speed = 350 rpm, T = 25±2°C)

Table 3. Comparison of the maximum adsorption capacity of F^- with different adsorbents.

Adsorbent	Q_e (mg g^{-1})	Reference
Al^{3+} pretreated low-silica synthetic zeolites	28.21–41.35	77
Hardened alumina cement	34.36	78
Zirconium impregnated coconut fiber carbon	40.016	79
Aluminum-Impregnated chitosan Biopolymer	1.73	80
Nano-alumina	14	81
Aluminium hydroxide impregnated macroreticular	36.61	82
Aluminum-based adsorbent	**43.29**	**This study**

The equilibrium data were further processed using Langmuir and Freundlich isotherms. The Langmuir model is based on the hypothesis that uptake occurs on a homogenous surface by monolayer adsorption without interaction between adsorbed molecules. While the Freundlich model proposes multilayer adsorption with a heterogeneous energetic distribution of active sites and with the interaction between adsorbed molecules. The Langmuir and Freundlich adsorption isotherms for the F^- adsorption are presented in Figure 12.

Langmuir and Freundlich adsorption isotherm constants are indicated in Table 3.

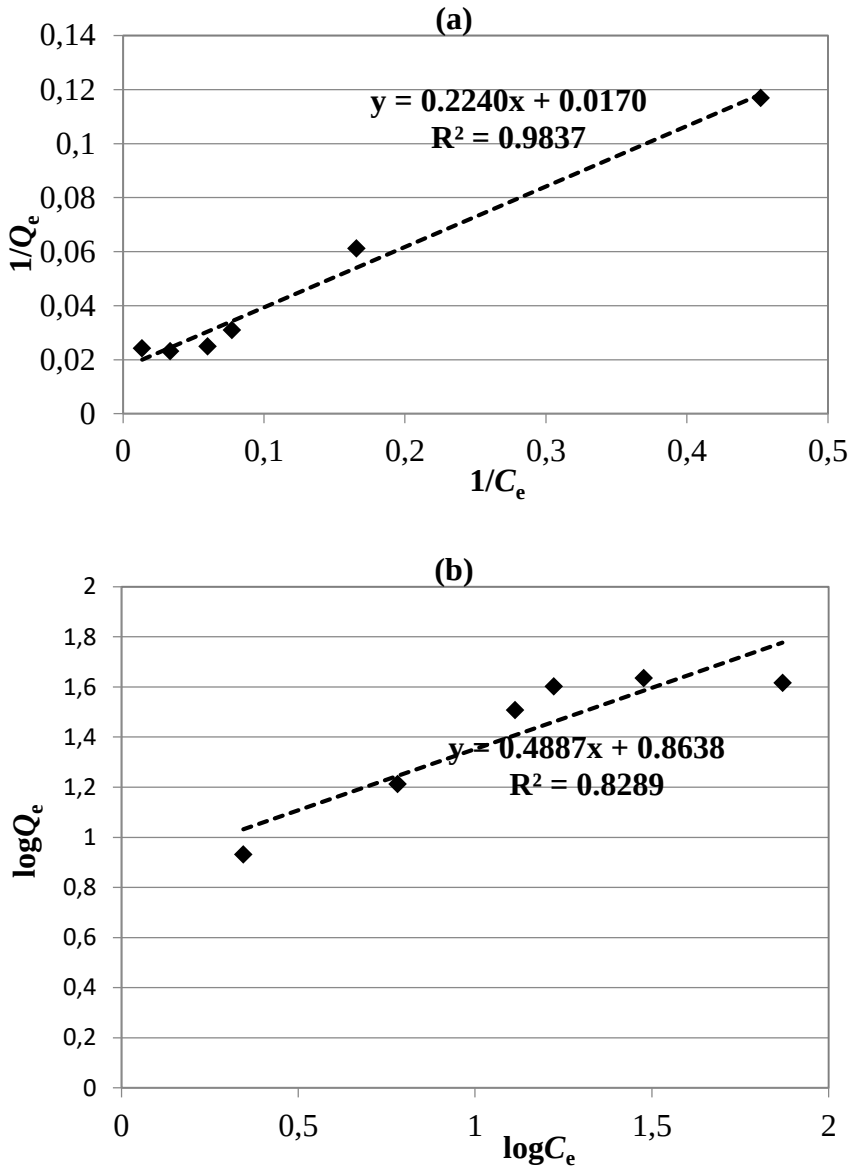

Figure 12. Langmuir (a) and Freundlich (b) isotherm plots for F^- adsorption (adsorbent dose = 3 g L^{-1}, natural pH = 7±0.2, contact time = 24 h, initial F^-concentration = 20-160 mg L^{-1}, agitation speed = 350 rpm, T = 25±2°C)

Table 3. Langmuir and Freundlich adsorption isotherm constants.

Langmuir			**Freundlich**		
Q_m (mg g^{-1})	**K_L (L mg^{-1})**	**R^2**	***n***	**K_F**	**R^2**
58.82	0.076	0.9837	2.046	0.1368	0.8289

The essential features of the Langmuir isotherm can be expressed by the equilibrium parameter (R_L) which is determined by the Eq. (11) [83].

$$R_L = \frac{1}{1+K_L C_0} \quad (11)$$

Where C_0 (mg L^{-1}) is the initial concentration of F^- and K_L (L mg^{-1}) is the Langmuir constant related to the energy of adsorption. The value of R_L indicates the shape of the isotherms to be either unfavourable (R_L > 1), linear (R_L = 1), favourable (0 < R_L <1) or irreversible (R_L = 0). The calculated R_L values as different initial fluoride concentrations are shown in Figure 13. It was observed that the value of R_L in the range 0-1 confirms the favourable adsorption.

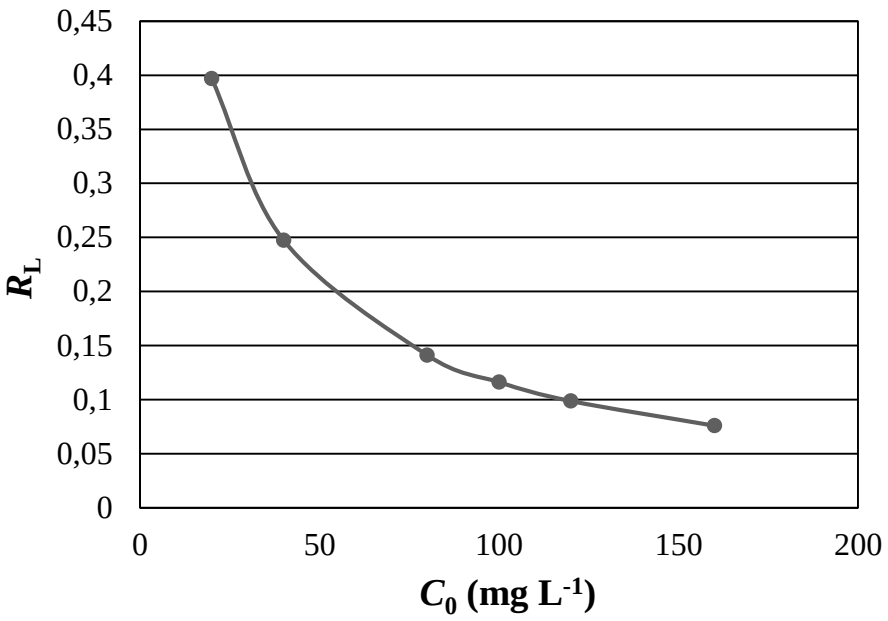

Figure 13. Plot of equilibrium parameter versus initial fluoride concentration.

The favourable adsorption of the Freundlich isotherm can be characterised such that if a value for *n* is above unity, adsorption is favourable and a physical process. In this study, the value of *n* (*n* = 2.046) is greater than 1, indicating that the adsorption is favourable. However, the value of correlation coefficient (R^2 = 0.8289) is lower than the Langmuir isotherm value (0.9837). Therefore, the F^- adsorption onto aluminium-based adsorbent were better described by Langmuir isotherm confirming monolayer adsorption without interaction between adsorbed molecules.

4. Conclusion

The defluoridation efficiency of aluminum-based adsorbent was evaluated in a batch adsorption reactor at room temperature (25±2°C). The results of the batch adsorption experiments demonstrated that 24 h of contact time between the adsorbent and the fluoride solution was sufficient to achieve equilibrium. It was observed that the maximum wastewater (84.91%) was obtained for 40 mg $L^{-1}$and 3 g L^{-1} of initial F^- concentration and adsorbent dose, respectively. It is worth noting that the percentage of F^- removal does not weaken in the wide pH range of 3 to 11. The adsorption of the F^- ions on the synthetic adsorbent is thus not dependent on pH. Kinetic studies revealed that F^- adsorption fitted well to pseudo-second-order model indicating the fluoride adsorption mechanism of aluminum-based adsorbent was of chemisorption type.

Furthermore, the adsorption isotherm of F^- sorption indicated that the maximum adsorption capacity of this latter was noted to be 43.29 mg g^{-1}. The experimental data indicated that the Langmuir isotherm was a suitable model for describing the F^- adsorption because of its high correlation coefficient.

According to the Langmuir concept, the adsorption of F^- onto aluminium-based adsorbent was monolayer adsorption with homogenous distribution of active sites and without interaction between adsorbed molecules. The obtained results indicated that the ion exchange is probably the primary mechanism involved. This study indicated that aluminum-based adsorbent is an efficient material for the removal of fluoride from aqueous solutions, which can be used in water treatment without any additional modification. However, its widespread use is restricted due to high cost. Thus, the search for natural materials such as clays can be an up-and-coming alternative.

Nomenclature

C_0 Initial F^- concentrations (mg L^{-1})
C_e Equilibrium concentrations of F^- (mg L^{-1})
K_{ad} Rate constant (min^{-1})
K_F Freundlich constants related to adsorption capacity (mg g^{-1})
K_1 Pseudo-first order rate constant (min^{-1})
K_2 Pseudo-second order rate constant (g mg^{-1} min^{-1})
n Adsorption intensity (heterogeneity factor)
Q_t Amount of F^- adsorbed per unit mass of adsorbent at time *t*
Q_e Equilibrium adsorbate capacity (mg.g^{-1})
V Volume of the aqueous solution (mL)
W Mass of adsorbent (g)
R_L Equilibrium parameter

References

1- N. Mondillo, M. Boni, G. Balassone, S. Spoleto, F. Stellato, A. Marino, L. Santoro, J. Spratt, Rareearth elements minerals in the silius fluorite vein system (sardinia, italy), Ore Geol. Rev., **2016**, 74, 211-224.

2- S.S. Tripathy, J.L. Bersillon, K. Gopal, Removal of fluoride from drinking water by adsorption onto alum-impregnated activated alumina, Sep. Purif. Technol., **2006**, 50, 310-317.
3- D.E. Yerien, S. Bonesi, A. Postigo, Fluorination methods in drug discovery, Org. Biomol. Chem., **2016**, 14, 8398-8427.
4- Y.P. Xiao, J. Zhang, Y.H. Liu, J.H. Zhang, Q.Y. Yu, Z. Huang, X.Q. Yu, Low molecular weight PEI-based fluorinated polymers for efficient gene delivery, Eur. J. Med. Chem., **2019**, 162, 602-611.
5- I. Kaur, B.N. Misra, A. Kohli, Synthesis of Teflon-FEP grafted membranes for use in water desalination, Desalination, **2001**, 139, 357-365.
6- K.S. Oh, W. Bae, H. Kim, Dispersion polymerization of N-vinylcarbazole using siloxane-based and fluorine-based surfactants in compressed liquid dimethyl ether, Polymer, **2007**, 48, 1450-1454.
7- S. Sasamoto, H. Suzuki, Fluorine-based surfactant, and coating composition and resist composition each using the same, US20130172476A1, **2013**.
8- M. Mohapatra, K. Rout, P. Singh, S. Anand, S. Layek, H.C. Verma, B.K. Mishra, Fluoride adsorption studies on mixed-phase nano iron oxides prepared by surfactant mediation-precipitation technique, J. Hazard. Mater., **2011**, 186, 1751-1757.
9- J. Dai, Stable electrolytes for high voltage batteries and the batteries derived therefrom, US20110200864A1, **2011**.
10- A. Ghosh, K. Mukherjee, S.K. Ghosh, B. Saha, Sources and toxicity of fluoride in the environment, Res. Chem. Intermed., **2013**, 39, 2881-2915.
11- L. Deng, Y. Liu, T. Huang, T. Sun, Fluoride removal by induced crystallization using fluorapatite/calcite seed crystals, Chem. Eng. J., **2016**, 287, 83-91.
12- D.L. Ozsvath, Fluoride and environmental health: a review, Rev. Environ. Sci. Biotechnol., **2009**, 8, 59-79.
13- S. Raghav, D. Kumar, Adsorption equilibrium, kinetics, and thermodynamic studies of fluoride adsorbed by tetrametallic oxide adsorbent, J. Chem. Eng. Data., **2018**, 63, 1682-1697.
14- C.Y. Hu, S.L. Lo, W.H. Kuan, Y.D. Lee, Removal of fluoride from semiconductor wastewater by electrocoagulation–flotation, Water Res., **2005**, 39, 895-901.
15- H. Huang, J. Liu, P. Zhang, D. Zhang, F. Gao, Investigation on the simultaneous removal of fluoride, ammonia nitrogen and phosphate from semiconductor wastewater using chemical precipitation, Chem. Eng. J., **2017**, 307, 696-706.
16- K. Van den Broeck, N. Van Hoornick, J. Van Hoeymissen, R. de Boer, A. Giesen, D. Wilms, Sustainable treatment of HF wastewaters from semiconductor industry with a fluidized bed reactor, IEEE Trans. Semicond. Manuf., **2003**, 16, 423-428.
17- N. Zhang, X. Xiao, H. Pang, Transition metal (Fe, Co, Ni) fluoride-based materials for electrochemical energy storage, Nanoscale Horiz., **2019**, 4, 99-116.
18- C.-X. Zu, H. Li, Thermodynamic analysis on energy densities of batteries, Energy Environ. Sci., **2011**, 4, 2614.
19- A.M.H.R. Hasan, S.K. Sidhu, J.W. Nicholson, Fluoride release and uptake in enhanced bioactivity glass ionomer cement ("glass carbomerTM") compared with conventional and resin-modified glass ionomer cements, J. Appl. Oral Sci., **2019**, 27. http://dx.doi.org/10.1590/1678-7757-2018-0230 .
20- R.S. Quimby, M. Saad, Pathways to a 4 μm Dy^{3+} Fluoride Glass Fiber Laser, in: Lasers Congr. 2016 ASSL LSC LAC, OSA, Boston, Massachusetts, **2016**, 2A-34.
21- J.A. Camargo, Fluoride toxicity to aquatic organisms: a review, Chemosphere, **2003**, 50, 251-264.
22- M.A. Karami, Y. Fakhri, S. Rezania, A.A. Alinejad, A.A. Mohammadi, M. Yousefi, M. Ghaderpoori, M.H. Saghi, M. Ahmadpour, Non-carcinogenic health risk assessment due to fluoride exposure from tea consumption in iran using monte carlo simulation, Int. J. Environ. Res. Public Health, **2019**, 16, 4261.
23- S. Raghava, D. Kumara, Comparative kinetics and thermodynamic studies of fluoride adsorption by two novel synthesized biopolymer composites, Carboh Poly., **2019**, 203, 430–440.
24- M. Yousefi, S. Ghalehaskar, F.B. Asghari, A. Ghaderpoury, M.H. Dehghani, M. Ghaderpoori, A.A. Mohammadi, Distribution of fluoride contamination in drinking water resources and health risk assessment using geographic information system, northwest Iran, J. Reg. Toxicol. Pharm., **2019**, 107, 104408.
25- S. Gupta, A.N. Poddar, Sodium fluoride toxicity in the fresh water cat fish clarias batrachus (linn.): effects on the erythrocyte morphology and antioxidant enzymes, Res. J. Environ. Toxicol., **2014**, 8, 68-76.
26- A. Dhillon, S. Nehra, D. Kumar, Dual adsorption behaviour of fluoride from drinking water on Ca-$Zn(OH)_2CO_3$ adsorbent, J. Surf. In., **2017**, 6, 154-161.
27- M. Ghaderpoori, M. Paydar, A. Zarei, H. Alidadi, A.A. Najafpoor, A.H. Gohary, M. Shams, Health risk assessment of fluoride in water distribution network of Mashhad, Iran, Human and Ecological Risk Assessment: An International Journal, **2019**, 25, 851-862.
28- M. Radfard, M. Rahmatinia, H. Akbari, B. Hashemzadeh, H. Akbari, A. Adibzadeh, Data on health risk assessment of fluoride in water distribution network of Iranshahr, Iran, J. Data. Brief., **2018**, 20, 1446–1452.

29- B.L. Riggs, S.F. Hodgson, W.M. O'Fallon, E.Y.S. Chao, H.W. Wahner, J.M. Muhs, S.L. Cedel, L.J. Melon, Effect of fluoride treatment on the fracture rate in postmenopausal women with osteoporosis, N. Engl. J. Med., **1990**, 322, 802-809.
30- J. Li, Q. Zhao, Y. Li, Y. Bao, B. Li, H. Yan, S. Huo, Y. Fan, Y. Yang, Y. Gao, Effects of embryonic exposure to fluoride on bone development of zebrafish, Chin. J. Endem., **2018**, 37, 24-29.
31- P.T.C. Harrison, Fluoride in water: A UK perspective, J. Fluor. Chem., **2005**, 126, 1448-1456.
32- Y. Zhou, C. Yu, Y. Shan, Adsorption of fluoride from aqueous solution on La^{3+} impregnated cross-linked gelatin, Sep. Purif. Technol., **2004**, 36, 89-94.
33- J. Fawell, K. Bailey, J.Chilton, E. Dahi, Y. Magara, Fluoride in drinking- water the first edition, London, UK, IWA publishing, **2006**, 97-126.
34- H. Rezaei, A. Jafari, B. Kamarehie, Y. Fakhri, Af. Ghaderpoury, M.A. Karami, M.Ghaderpoori, M. Shams, F. Bidarpoor, M. Salimi, Health-risk assessment related to the fluoride, nitrate, and nitrite in the drinking water in the Sanandaj, Kurdistan County, Iran." Human and ecological risk assessment: an international journal, **2018**, 25, 1242-1250.
35- G.C. dos Santos Bazanella, G.F. da Silva, A.M.S. Vieira, R. Bergamasco, Fluoride removal from water using combined Moringa Oleifera/ultrafiltration process, Water. Air. Soil Pollut., **2012**, 233, 6083-6093.
36- M. Suneetha, B.S. Sundar, K. Ravindhranath, Removal of fluoride from polluted waters using active carbon derived from barks of Vitex negundo plant, J. Anal. Sci. Technol., **2015**, 6, 15.
37- L. Deng, X. Zhang, T. Huang, J. Zhou, Investigation of fluorapatite crystallization in a fluidized bed reactor for the removal of fluoride from groundwater: investigation of fluorapatite crystallization in a fluidized bed reactor for the removal, J. Chem. Technol. Biotechnol., **2019**, 94, 569-581.
38- N.S. Graça, A.M. Ribeiro, A.E. Rodrigues, Removal of fluoride from water by a continuous electrocoagulation process, Ind. Eng. Chem. Res., **2019**, 58, 5314-5321.
39- V.F. Mena, A. Betancor-Abreu, S. González, S. Delgado, R.M. Souto, J.J. Santana, Fluoride removal from natural volcanic underground water by an electrocoagulation process: parametric and cost evaluations, J. Environ. Manage., **2019**, 246, 472-483.
40- Y.-X. Zhang, Y. Jia, Fluoride adsorption on manganese carbonate: Ion-exchange based on the surface carbonate-like groups and hydroxyl groups, J. Colloid Interface Sci., **2018**, 510, 407-417.
41- N. Viswanathan, I.A. Kumar, S. Meenakshi, Development of chitosan encapsulated tricalcium phosphate biocomposite for fluoride retention, Int. J. Biol. Macromol., **2019**, 133, 811-816.
42- F. Shen, X. Chen, P. Gao, G. Chen, Electrochemical removal of fluoride ions from industrial wastewater, Chem. Eng. Sci., **2003**, 58, 987-993.
43- I. Owusu-Agyeman, M. Reinwald, A. Jeihanipour, A.I. Schäfer, Removal of fluoride and natural organic matter from natural tropical brackish waters by nanofiltration/reverse osmosis with varying water chemistry, Chemosphere, **2019**, 217, 47-58.
44- S. Parveen, V.N. Ratnakaram, S. Malladi, K. Kiram Kumar, Design of a Domestic Defluoridizing Unit, in: B. Subramanian, S.S. Chen, K.R. Reddy (Eds.), Emerg. Technol. Agric. Environ., Springer, Singapore, **2020**, 173-183.
45- X. Wang, N. Li, J. Li, J. Feng, Z. Ma, Y. Xu, Y. Sun, D. Xu, J. Wang, X. Gao, J. Gao, Fluoride removal from secondary effluent of the graphite industry using electrodialysis: Optimization with response surface methodology, Front. Environ. Sci. Eng., **2019**, 13, 51.
46- N. Arahman, S. Mulyati, M.R. Lubis, R. Takagi, H. Matsuyama, The removal of fluoride from water based on applied current and membrane types in electrodialysis, J. Fluor. Chem., **2016**, 191, 97-102.
47- G. Yan, Y. Bao, M. Tan, Q. Cui, X. Lu, Y. Zhang, Defluorination by Donnan Dialysis with seawater for seafood processing, J. Food Eng., **2018**, 238, 22-29.
48- S.I. Bouhadjar, H. Kopp, P. Britsch, S.A. Deowan, J. Hoinkis, J. Bundschuh, Solar powered nanofiltration for drinking water production from fluoride-containing groundwater A pilot study towards developing a sustainable and low-cost treatment plant, J. Environ. Manage., **2019**, 231, 1263-1269.
49- G. Crini, E. Lichtfouse, Advantages and disadvantages of techniques used for wastewater treatment, Environ. Chem. Lett., **2019**, 17, 145-155.
50- L.S. Thakur, P. Mondal, Simultaneous arsenic and fluoride removal from synthetic and real groundwater by electrocoagulation process: Parametric and cost evaluation, J. Environ. Manage., **2017**, 190, 102-112.
51- M. Sarkar, A. Banerjee, P.P. Pramanick, A.R. Sarkar, Use of laterite for the removal of fluoride from contaminated drinking water, J. Colloid Interface Sci., **2006**, 302, 432-441.
52- A. Ndé-Tchoupé, R. Crane, H. Mwakabona, C. Noubactep, K. Njau, Technologies for Decentralized Fluoride Removal: Testing Metallic Iron-based Filters, Water, **2015**, 7, 6750-6774.
53- H. Wang, Q. Feng, K. Liu, Z. Li, X. Tang, G. Li, Highly efficient fluoride adsorption from

aqueous solution by nepheline prepared from kaolinite through alkali-hydrothermal process, J. Environ. Manage., **2017**, 196, 72-79.
54- M.T. Hadjyoussef, M. Jendoubi, M.B. Amor, Removal of Fluoride from drinking water by an activated Bentonite: application to a drinking Tunisian water, Mor. J. Chem., **2018**, 6, 135-147.
55- K. Kulkarni, G.M. Bhogale, R. Nalawade, Adsorptive removal of fluoride from water samples using Azospirillum biofertilizer and lignite, Korean J. Chem. Eng., **2018**, 35, 153-163.
56- L. Deng, Y. Liu, T. Huang, T. Sun, Fluoride removal by induced crystallization using fluorapatite/calcite seed crystals, Chem. Eng. J., **2016**, 287, 83-91.
57- M. Mourabet, A. El Rhilassi, H. El Boujaady, M. Bennani-Ziatni, R. El Hamri, A. Taitai, Removal of fluoride from aqueous solution by adsorption on Apatitic tricalcium phosphate using Box–Behnken design and desirability function, Appl. Surf. Sci., **2012**, 258, 4402-4410.
58- J.P. Maity, C.-M. Hsu, T.-J. Lin, W.-C. Lee, P. Bhattacharya, J. Bundschuh, C.-Y. Chen, Removal of fluoride from water through bacterial-surfactin mediated novel hydroxyapatite nanoparticle and its efficiency assessment: adsorption isotherm, adsorption kinetic and adsorption Thermodynamics, Environ. Nanotechnol. Monit. Manag., **2018**, 9, 18-28.
59- A. Vinati, E.R. Rene, K. Pakshirajan, S.K. Behera, Activated red mud as a permeable reactive barrier material for fluoride removal from groundwater: parameter optimisation and physico-chemical characterisation, Environ. Technol., **2019**, 6, 1-12.
60- M. Dessalegne, F. Zewge, W. Mammo, G. Woldetinsae, I. Diaz, Effective fluoride adsorption by aluminum oxide modified clays: Ethiopian bentonite vs commercial montmorillonite, Bull. Chem. Soc. Ethiop., **2018**, 32, 199-211.
61- S.S. Tripathy, J.-L. Bersillon, K. Gopal, Removal of fluoride from drinking water by adsorption onto alum-impregnated activated alumina, Sep. Purif. Technol., **2006**, 50, 310-317.
62- V.K. Gupta, Suhas, Application of low-cost adsorbents for dye removal-A review, J. Environ. Manage., **2009**, 90, 2313-2342.
63- U. Kumari, S.K. Behera, B.C. Meikap, A novel acid modified alumina adsorbent with enhanced defluoridation property: Kinetics, isotherm study and applicability on industrial wastewater, J. Hazard. Mater., **2019**, 365, 868-882.
64- D.-C. Shin, S.S. Park, J.H. Kim, S.S. Hong, J.M. Park, S.H. Lee, D.S. Kim, G.D. Lee, Study on α-alumina precursors prepared using different ammonium salt precipitants, Journal of Industrial and Engineering Chemistry, **2014**, 20, 1269-1275.
65- NF T 90-004: Water quality – Determination of fluoride ion-Potentiometric method, **2002**.
66- A. Dhillon, S.K. Soni, D. Kumar, Enhanced fluoride removal performance by Ce-Zn binary metal oxide : Adsorption characteristics and mechanism, J. Fluo. Chem., **2017**, 199, 67-76.
67- K.G. Bhattacharyya, S.S. Gupta, Influence of acid activation on adsorption of Ni(II) and Cu(II) on kaolinite and montmorillonite: kinetic and thermodynamic study, Chemical Engineering Journal, **2008**, 136, 1-13.
68- E.I. Unuabonah, K.O. Adebowale, B.-I. Olu-Owolabi, Kinetic and thermodynamic studies of the adsorption of lead (II) ions onto phosphate-modified kaolinite clay, Journal of Hazardous Materials, **2007**, 144, 386-395.
69- I. Langmuir, The constitution and fundamental properties of solids and liquids, J. Ameri Chem Soci., **1916**, 38, 2221-2295.
70- H.M.F. Freundlich, Over the adsorption in solution, The Journal of Physical Chemistry, **1906**, 57, 385-471.
71- N. Drouiche, S. Aoudj, M. Hecini, N. Ghaffour, H. Lounici, N. Mameri, Study on the treatment of photovoltaic wastewater using electrocoagulation: Fluoride removal with aluminium electrodes-Characteristics of products. J. Hazard. Mat., **2009**, 169, 65-69.
72- L. M. Weinstock, J.M. Stevenson, S.A. Tomellin, S.H. Pan, T. Utne, R.B. Jobson, D.F. Reinhold, Characterization of the actual catalytic agent in potassium fluoride on activated alumina systems. Tetrahedron Letters, **1986**, 27, 3845–3848.
73- K.G. Akpomie, A.F. Dawodu, K.O. Adebowale, Mechanism on the sorption of heavy metals from binary-solution by a low-cost montmorillonite and its desorption potential, Alexandria Enginering Journal, **2015**, 54, 757-767.
74- M. Massoudinejad, S.M. Mohsenib, M. Ghaderpoori, M. Sarkhosh, Soleyman Sahebi, Improvement of montmorillonite adsorption capacity for lead ions by modifying with hexadecyl trimethyl ammonium chloride: Characterization, modelling and optimization studies, MethodsX, **2019**, 6, 2217–2229.
75- K. Sakurai, Y. Ohdate, K. Kyuma, Comparison of salt titration and potentiometric titration methods for the determination of Zero Point of Charge (ZPC), Soil scien. Plant. Nutrition, **1988**, 34, 171-182.
76- S.H. Tan, N.A. Ismail, Isotherm and kinetic studies of L-phenylalanine adsorption onto porous nanosilica, Materials, today: Proceeding, **2018**, 5, 3193-3201.
77- M.S. Onyango, Y. Kojima, A. Kumar, D. Kuchar, M. Kubota, H. Matsuda Uptake of fluoride by Al^{3+} pretreated low-silica synthetic zeolites: Adsorption equilibrium and rate studies, Sep. Sci. Technol., **2006**, 41, 683-704.
78- S. Ayoob, A.K. Gupta, Insights into isotherm making in the sorptive removal of fluoride from drinking water, J. Hazard. Mater., **2008**, 152, 976-985

79- R.S. Sathish, S. Sairam, V.G. Raja, G.N. Rao, C. Janardhana Defluoridation of water using zirconium impregnated coconut fiber carbon, Sep. Sci. Technol., **2008**, 43, 3676-3694.
80- S.K. Swain, R.K. Dey, M. Islam, R.K. Patel, U. Jha, T. Patnaik, C. Airoldi Removal of fluoride from aqueous solution using aluminum-impregnated chitosan biopolymer, Sep. Sci. Tech., **2009**, 44, 2096-2116.
81- E. Kumar, A. Bhatnagar, U. Kumar, M. Sillanpää, Defluoridation from aqueous solutions by nano-alumina: Characterization and sorption studies, J. Hazard. Mater., **2011**, 186, 1042-1049.
82- M. Barathi, A. S. K. Kumar, N. Rajesh, Aluminium hydroxide impregnated macroreticular aromatic polymeric resin as a sustainable option for defluoridation, J. Environ Chem. Eng., **2015**, 3, 630-641
83- B. Meroufel, O. Benali, M. Benyahia, Y. Benmoussa, M.A. Zenasni, Adsorptive removal of anionic dye from aqueous solutions by Algerian kaolin: Characteristics, isotherm, kinetic and thermodynamic studie, J. Mater. Environ. Sci., **2013**, 4, 482-491.